

Chapter 3

Theoretical Background of Photophysical Properties



Kazuyuki Ishii  and Masako Kato 

Abstract In this chapter, we aim to explain the chromic phenomena observed in “soft crystals”. Accordingly, the basic principles for comprehending the fundamental photophysical properties of molecular monomers, such as electronic absorption spectra and luminescence properties, are introduced. Moreover, the photophysical properties of molecular dimers and molecular crystals are explained in terms of intermolecular interactions in excited states.

Keywords Soft crystals · UV-vis absorption · Luminescence · Photophysical properties

3.1 Background and Significance

Color and/or luminescence color changes, called chromism, with structural changes in molecular crystals are one of essential characteristics of soft crystals [1]. In recent decades, in the case of molecular monomers, theoretical quantum calculations have been developed to be able to reproduce the photophysical properties experimentally evaluated. On the other hand, although Davydov splitting, which results from exciton interactions, has long been recognized as the important photophysical property of molecular crystals [2], even at this stage, it is difficult to comprehend the photophysical properties of molecular crystals using similar approaches. This originates from the coexistence of intramolecular interactions based on strong interatomic bonds and non-negligible electronic intermolecular interactions in molecular crystals, which are different from the molecular monomers or inorganic crystals. In this chapter, molecular photophysical properties are explained in terms of molecular monomers,

K. Ishii (✉)

Institute of Industrial Science, The University of Tokyo, 4-6-1 Komaba, Meguro-Ku,
Tokyo 153-8505, Japan
e-mail: k-ishii@iis.u-tokyo.ac.jp

M. Kato

Department of Applied Chemistry for Environment, Kwansai Gakuin University, 1 Gakuen
Uegahara, Sanda 669-1330, Japan
e-mail: katom@kwansai.ac.jp

© The Author(s) 2023

M. Kato and K. Ishii (eds.), *Soft Crystals*, The Materials Research Society Series,
https://doi.org/10.1007/978-981-99-0260-6_3

dimers, and crystals. First, we explain the basic photophysical properties of molecular monomers, such as electronic absorption spectra, fluorescence and phosphorescence spectra, luminescence lifetimes, and luminescence yield, focusing on the π - π^* and metal-to-ligand charge transfer (MLCT) excited states, which are essential for the chromism of organic molecules and metal complexes. Next, the photophysical properties of molecular dimers are briefly described using intermolecular interactions, such as exciton interactions and charge transfer interactions, in addition to metal-metal-to-ligand charge transfer which are crucial in soft crystals based on metal complexes. Finally, we introduce the theoretical analysis on photoconductive molecular crystals using exciton and charge transfer interactions.

3.2 Photophysical Properties of Diamagnetic Molecular Monomers

This chapter focuses on the photophysical properties of molecules showing diamagnetism in the ground state, which are the majority of luminescent organic molecules and metal complexes.

Figure 3.1 depicts the photophysical processes occurring in diamagnetic molecules [3]. Here, the singlet ground (S_0) state, the lowest excited singlet (S_1) state, and the lowest excited triplet (T_1) state are considered. Although the actual excited states are represented as a result of configuration interaction between several excited configurations, the S_1 and T_1 states are approximately represented here as the transition states from the highest occupied molecular orbital (HOMO) to the lowest unoccupied molecular orbital (LUMO). The general photophysical processes are: (1) spin-allowed singlet-singlet (S_0 - S_n) absorption, (2) $S_1 \rightarrow S_0$ fluorescence, (3) $T_1 \rightarrow S_0$ phosphorescence, (4) spin-forbidden thermal deactivation processes, i.e., $S_1 \rightarrow T_1$ or $T_1 \rightarrow S_0$ intersystem crossing (ISC), and (5) spin-allowed thermal deactivation process i.e., $S_1 \rightarrow S_0$ internal conversion (IC). The detail procedures (1)-(4) are described in the following sections.

3.3 Electronic Absorption and Luminescence of π - π^* Transitions

In diamagnetic organic compounds and metal complexes containing metal ions with d^0 or d^{10} electron configuration, excited configurations, such as (π - π^*), (n - π^*), (σ - π^*), (π - σ^*), and (σ - σ^*), are considered. Because the σ (or σ^*) orbitals are highly stabilized (or destabilized), (σ - π^*), (π - σ^*), and (σ - σ^*) are typically observed in the UV region or higher energies region. Thus, the electronic absorption bands originating from (π - π^*) and (n - π^*) are frequently observed in the visible region. Because the molar absorption coefficient (ϵ) of (n - π^*) transitions is much smaller than that of

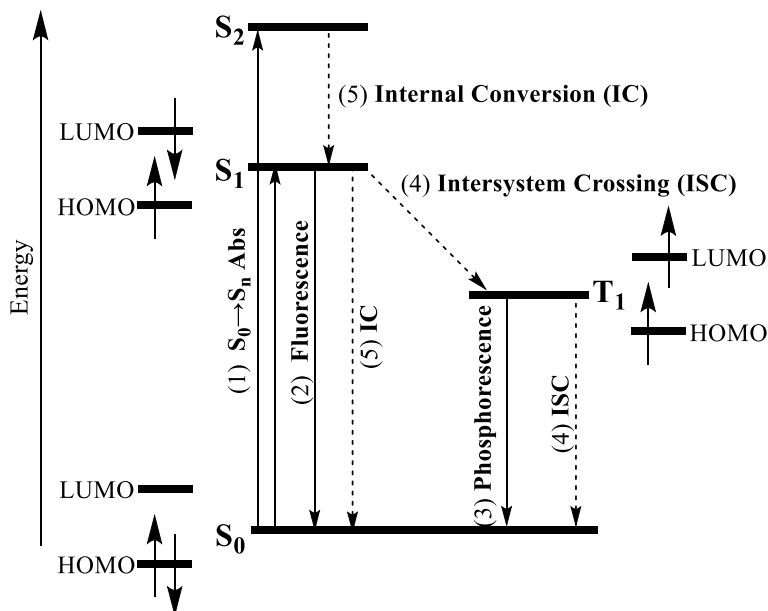


Fig. 3.1 Photophysical processes of a typical diamagnetic molecule

($\pi-\pi^*$) transitions, the ($\pi-\pi^*$) transitions are mainly responsible for the coloration of molecules. For metal complexes containing transition metal ions with the d^n ($n = 1-9$) electron configuration, the ($d-\pi^*$) (or MLCT) configuration is crucial. In this and the following sections, we discuss ($\pi-\pi^*$) and MLCT, using phthalocyanines, which are practically used as blue or green dyes and pigments, as well as for photoconducting materials in laser-beam printers and photocopiers [4].

Figure 3.2 depicts the electronic absorption, fluorescence, and phosphorescence spectra of a zinc phthalocyanine complex (the diamagnetic central metal is Zn^{2+} with the d^{10} electron configuration) showing a typical ($\pi-\pi^*$) transitions.

In the UV-vis spectrum, a sharp and strong absorption band attributed to the $S_0 \rightarrow S_1$ transition is seen at approximately 680 nm, which is called as the Q band. In contrast, the absorption band centered around 350 nm is referred to as the Soret band, which originates from the $S_0 \rightarrow S_2$ transition. These S_1 and S_2 states corresponding to $^1(\pi-\pi^*)$ consist primarily of $HOMO(\pi) \rightarrow LUMO(\pi^*)$ and $HOMO-1(\pi) \rightarrow LUMO(\pi^*)$, respectively (Fig. 3.3).

The electronic transition probability of a $S_0 \rightarrow S_n$ transition is expressed by the oscillator strength f , which is expressed to be proportional to the integral of the experimental absorption coefficient ϵ , as follows:

$$f_{S_n \leftarrow S_0} = 4.32 \times 10^{-9} \int \epsilon(\tilde{\nu}) d\tilde{\nu} \quad (3.1)$$

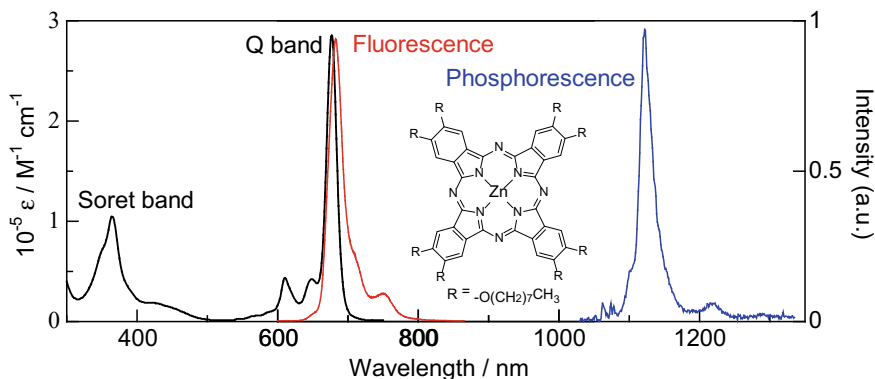
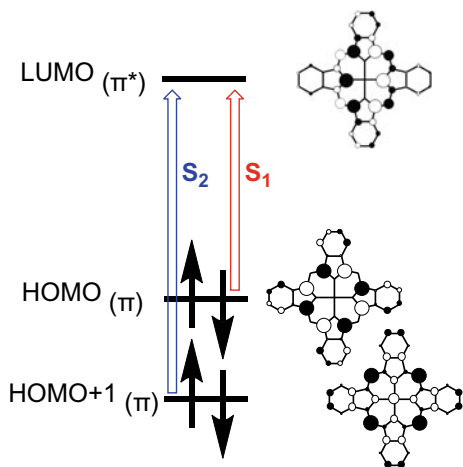


Fig. 3.2 UV-vis absorption (black line), fluorescence (red line), and phosphorescence (blue line) spectra of a zinc phthalocyanine complex [4]

Fig. 3.3 Four frontier π MOs of ZnPc. Only one LUMO is shown, although two LUMOs are degenerated for ZnPc



The oscillator strength f is expressed by the theoretically calculated electric dipole strength as follows.

$$f_{S_n \leftarrow S_0} = \left(\frac{8\pi^2 m_e \nu}{3he^2} \right) \left| \left\langle S_n \left| \sum_i e r_i \right| S_0 \right\rangle \right|^2 \quad (3.2)$$

The (π - π^*) transition is distinguished by the fact that ϵ is frequently large (10^3 – $10^5 \text{ M}^{-1} \text{ cm}^{-1}$) when it is the electric dipole allowed transition. For example, the ϵ value of the Q band of zinc(II) phthalocyanine is very large ($\sim 3 \times 10^5 \text{ M}^{-1} \text{ cm}^{-1}$). In addition, vibronic bands, which are based on the misalignment of the most stable structure between the ground and excited states and reflect the vibrational structures

in the excited state, can be observed because of the sharp absorption bands (the full width at half maximum (FWHM) of the Q band of zinc(II) phthalocyanine is 450 cm^{-1}).

As depicted in Fig. 3.2, the $S_1 \rightarrow S_0$ fluorescence of zinc(II) phthalocyanine is observed around 700 nm, which is the mirror image of the Q band. The peak difference (Stokes shift) between the absorption and fluorescence is small, which is characteristic of the $^1(\pi-\pi^*)$ transition and reflects the small structural change caused by photoexcitation. The phosphorescence of zinc(II) phthalocyanine is observed at approximately 1100 nm and 77 K, where non-radiative deactivation is suppressed.

Using the excited state lifetime (τ_F : fluorescence lifetime, τ_P : phosphorescence lifetime), luminescence efficiency (Φ_F : fluorescence quantum yield, Φ_P : phosphorescence quantum yield), and triplet yield (Φ_T), the excited state dynamics in the S_1 and T_1 states is experimentally defined as follows.

$$\tau_F = 1/(k_F + k_{IC} + k_{ISC}), \quad (3.3a)$$

$$\tau_P = 1/(k_P + k'_{ISC}), \quad (3.3b)$$

$$\Phi_F = k_F/(k_F + k_{IC} + k_{ISC}), \quad (3.3c)$$

$$\Phi_T = k_{ISC}/(k_F + k_{IC} + k_{ISC}), \quad (3.3d)$$

$$\Phi_P = \Phi_T \times k_P/(k_P + k'_{ISC}), \quad (3.3e)$$

where, k_F and k_P are the radiative decay rate constants in fluorescence and phosphorescence, k_{IC} is the internal conversion rate constant, and k_{ISC} and k'_{ISC} are the intersystem rate constants. When no compensation in the condensed system is considered, k_F is expressed as follows.

$$k_F = \left(\frac{v_F^2}{1.5} \right) f_{S_0 \rightarrow S_1}. \quad (3.4)$$

k_F is proportional to the oscillator strength, similarly to the electronic absorption coefficient ε . Therefore, the k_F value is high when the ε value is large. For instance, in the case of metal phthalocyanines (central metal/axial ligand = Mg, Al, Zn, Ga, Cd, In), the k_F value is less dependent on the central metal, since the fluorescence is derived from $(\pi-\pi^*)$ of the phthalocyanine ligand.

On the other hand, the main non-radiative decay process is the intersystem transition from the S_1 state to the T_1 state. The intersystem crossing is governed by the spin-orbit coupling on the central atom, and consequently the fluorescence is strongly dependent on the central atom. In terms of the periodic table, we compare the τ_F and Φ_F of phthalocyanines as an example, either unsubstituted or substituted with *tert*-butyl groups. In the case of phthalocyanine containing the first and second

periodic elements (central atoms = 2H, 2Li, Mg, Al, Si), τ_F is relatively long, ranging from 3.8 to 9.0 ns, and Φ_F is also high, ranging from 0.57 to 0.85. For the third periodic elements (central atom = Zn, Ga), τ_F and Φ_F decreases to 3.15–4.73 ns and 0.30–0.37, respectively. In addition, for the fourth-period elements (central atoms = Cd, In, and Sb), τ_F significantly becomes short (0.37–0.6 ns) and Φ_F significantly decreases (0.03–0.08). Since the spin–orbit coupling is stronger for heavier atoms, the reduction in τ_F and Φ_F for heavier atoms can be interpreted as a strengthening of the intersystem crossing.

In Mg, Zn, and Cd phthalocyanine complexes, since the spin–orbit coupling is not large, Phosphorescence has been observed with extremely low Φ_P ($<10^{-3}$) and primarily measured at low temperatures, such as 77 K. Also, their triplet lifetimes at room temperature are relatively long and approximately a few hundred μ s.

3.4 Electronic Absorption and Luminescence of ($d-\pi^*$) (= MLCT) Transitions

Next, we describe a summary of MLCT transitions. Figure 3.4 depicts the UV–vis absorption and room temperature phosphorescence spectra of RuPc(CO)(py) and RuPc(py)₂ [5].

Similar to ZnPc, RuPc(CO)(py) with CO as an axial ligand displays a sharp and strong Q band attributed to ($\pi-\pi^*$). In contrast, RuPc(py)₂ demonstrates a broad Q band, which can be explained by the admixture between ($d-\pi^*$) (= MLCT) and

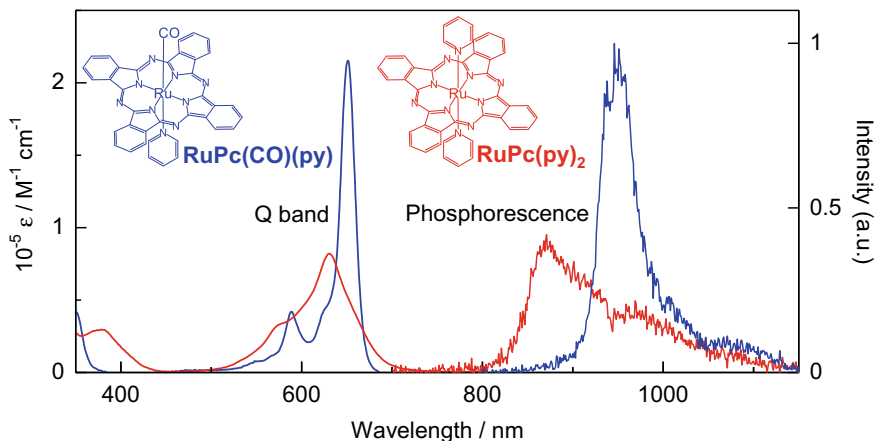


Fig. 3.4 UV-vis absorption and phosphorescence spectra of RuPc(CO)(py) (blue line) and RuPc(py)₂ (red line) at room temperature [5]. Here, four *tert*-butyl substituents in molecular structures are omitted for clarify

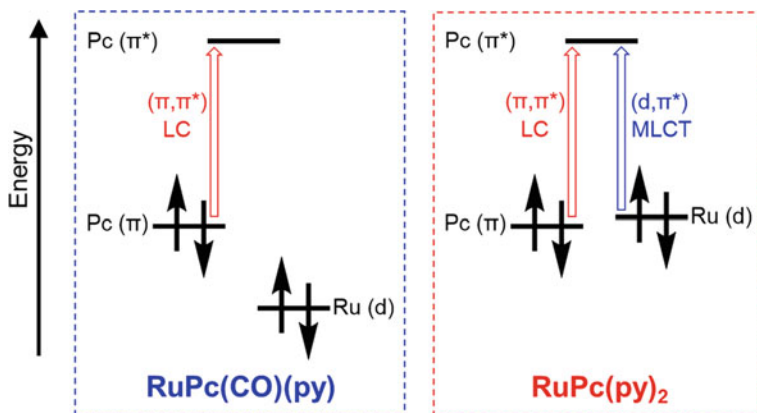


Fig. 3.5 Frontier MOs of RuPc(CO)(py) (left) and RuPc(py)₂ (right)

($\pi-\pi^*$) (= ligand center, LC). MLCTs are distinguished by a broad absorption bands and typically possess relatively large absorption coefficients ε ($10^3-10^4 \text{ M}^{-1} \text{ cm}^{-1}$).

The CO ligand is responsible for the distinction between RuPc(CO)(py) and RuPc(py)₂: CO is highly electron-withdrawing, and the π^* orbital of CO strongly interacts with the d_π orbital of the metal, stabilizing the d_π orbital of ruthenium to a greater extent than the π orbital of the Pc ligand (π -back donation). Consequently, the Q band attributed to ($\pi-\pi^*$) is observed in RuPc(CO)(py). On the other hand, in RuPc(py)₂, the energy of the d_π (Ru) orbital is of the same level as the π (Pc) orbital; thus, the MLCT contribution is more prominent (Fig. 3.5).

RuPc(CO)(py) and RuPc(py)₂ exhibit strong phosphorescence at room temperature. The T_1 state is attributed to ($\pi-\pi^*$) because of the sharp spectrum and relatively long lifetime (10 μs). In contrast, the phosphorescence spectrum of RuPc(py)₂ is broad and the phosphorescence lifetime is short (160 ns at 293 K), experimentally indicating that the MLCT contributes to the T_1 state as in the Q band.

Thus, metal phthalocyanine complexes containing second or third transition metal ions (especially those with d^6 or d^8 electron configuration) can exhibit efficient phosphorescence at room temperature; the phosphorescence radiation rate k_P between the T_1 and S_0 states can be expressed as follows.

$$k_P \propto \left| \langle \Phi_{S_0}^N | \Phi_{T_1}^N \rangle \right|^2 \left(\left| \langle \Phi_{S_n}^{ES} | \sum_k \sum_i \xi_{ki} l_i s_i | \Phi_{T_1}^{ES} \rangle \right|^2 / (E(S_n) - E(T_1)) \right) \left| \langle \Phi_{S_0} | \sum_i e r_i | \Phi_{S_n} \rangle \right|^2, \quad (3.5)$$

where, $E(S_n)$ and $E(T_1)$ are the energies of S_n and T_1 , respectively, $\left| \langle \Phi_{S_n}^{ES} | \sum_k \sum_i \xi_{ki} l_i s_i | \Phi_{T_1}^{ES} \rangle \right|^2$ is the spin-orbit coupling (SOC) between the T_1 and S_n states, and $\left| \langle \Phi_{S_0} | \sum_i e r_i | \Phi_{S_n} \rangle \right|^2$ is the transition electric dipole moment between the S_n and S_0 states. In other words, the phosphorescence gains intensity by borrowing the

transition electric dipole moment between the S_n and S_0 states via the SOC between the T_1 and S_n states. In the case of the second or third transition metal ions, the SOC constant, ξ , is large, causing high k_P and room temperature phosphorescence.

3.5 Photophysical Properties of Molecular Dimers

In molecular crystals, their photophysical properties are relatively complex because of the coexistence of strong interatomic bonds in molecules and non-negligible intermolecular electronic interactions. Therefore, firstly, we describe the photophysical properties of molecular dimers as a model in terms of intermolecular electronic interactions.

When considering the photophysical properties of molecular dimers, there are two types of methods, as in the case of molecular hydrogen: (1) the Valence Bond (VB) method, which first constructs the excited states of the consisting monomer units and then considers the interaction between units [6]. (2) the Molecular Orbital (MO) method, which considers the molecular orbitals of the dimer itself and its excited states [7]. The VB method can easily visualize the interaction between units, whereas the MO method can accurately represent the interactions when the interaction is substantial. These two methods are different from the viewpoint of starting points, but should provide similar results under the same approximations. In this section, we will discuss the exciton and charge-transfer interactions under the VB method using the phthalocyanine dimer as a model, as well as the metal–metal-to-ligand charge transfer (MMLCT) state under the MO method using Pt diimine complexes [8].

Using the phthalocyanine dimer as an example, we discuss the basic theory of homodimers composed of the same monomer units. The UV–vis absorption spectra of monomer and dimer of silicon phthalocyanine are depicted in Fig. 3.6 [9]. As compared to the monomer, the Q band of the dimer shifts to the blue-side (a shift to higher energy). This blue shift can be explained by the energy-transfer type, exciton interaction between two phthalocyanine units. Figure 3.7 illustrates the relationship between the dimeric configurations and exciton interactions. The energy splitting caused by the exciton interaction is approximately proportional to the transition electric dipole moment, and therefore, the exciton interaction is crucial in the phthalocyanine dimers because the Q band of phthalocyanines has a large transition electric dipole moment, as mentioned in Sect. 3.1.

In the case of a face-to-face type dimer, the excited state is destabilized when the transition electric dipoles are aligned in the same direction, while it is stabilized when the transition electric dipoles are aligned in the opposite direction. Thus, the transition from the S_0 state to the high-energy exciton state is allowed because of the sum of two transition electric dipoles, whereas the transition to the low-energy exciton state is forbidden.

For the head-to-tail type dimer, the transition to the high-energy exciton state is forbidden, whereas the transition to the low-energy exciton state is allowed. The transitions to the high-energy exciton and low-energy exciton states are allowed to

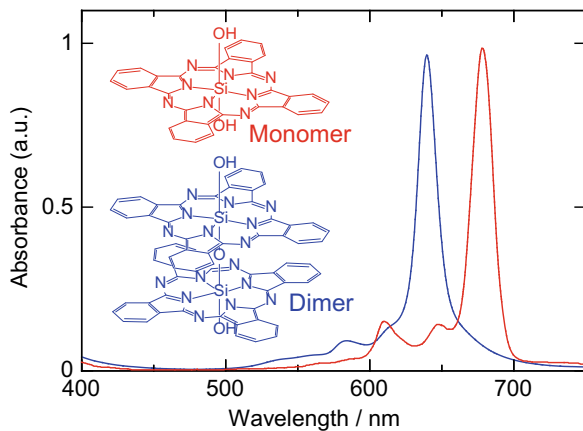


Fig. 3.6 UV-vis absorption spectra of the SiPc monomer (red line) and dimer (blue line) [9]. Here, four *tert*-butyl substituents in the molecular structures are omitted for clarity

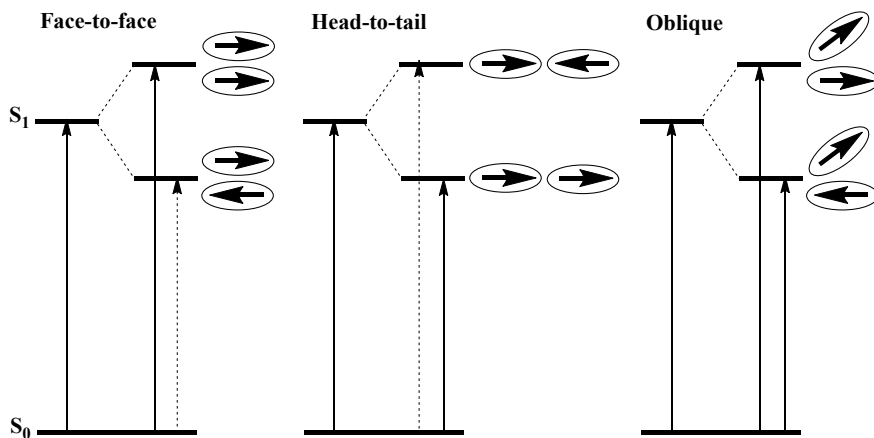


Fig. 3.7 Exciton interactions in various dimeric configurations

some extent for the oblique dimer, but their intensity is dependent on the dihedral angle of the Pc plane. The dimeric configuration can be estimated by analyzing its absorption spectrum based on this principle.

The electronic configuration describing the exciton interaction can be expressed as follows.

$$\Phi_{\text{EX}}(\pm) = (\varphi_A^* \varphi_B \pm \varphi_A \varphi_B^*) / \sqrt{2}, \quad (3.7)$$

where φ_A^* indicates the A unit in the S_1 (or T_1) state, and the + and - signs indicate the two exciton states.

In the face-to-face dimer, when the distance between constituting units is less than approximately the sum of the van der Waals radii, the low-energy exciton state significantly shifts to the red-side in comparison to the blue-shift of the high-energy exciton state. For instance, the SiPc dimer depicted in Fig. 3.6 exhibits a significant red-shifted fluorescence peak near 940 nm [9]. This large red-shift of over 200 nm cannot be explained only by the exciton interaction. Accordingly, it is explained by the contribution of the charge-transfer interactions in terms of the VB method. The electronic configuration of the charge resonance that reflects the charge transfer interaction can be described as follows.

$$\Phi_{\text{CR}}(\pm) = (\varphi_{\text{A}}^+ \varphi_{\text{B}}^- \pm \varphi_{\text{A}}^- \varphi_{\text{B}}^+) / \sqrt{2}, \quad (3.8)$$

where φ_{A}^+ and φ_{A}^- denote the A units in the cationic and anionic states, respectively. When the distance between the constituting units is short, the exciton and charge resonance configurations can be mixed, the wavefunction of the excited state of the dimer is expressed as

$$\Phi_{\text{DM}}(\pm) = \Phi_{\text{EX}}(\pm) + \Phi_{\text{CR}}(\pm). \quad (3.9)$$

The interaction with the energetically higher charge resonance configuration results in a substantial red-shift of the low-energy exciton state. Such a significant red-shift owing to dimerization is observed not only in the $S_1 \rightarrow S_0$ fluorescence, but also in the $T_1 \rightarrow S_0$ phosphorescence.

The exciton interactions are incredibly essential when the constituting dyes in the dimer have large transition electric dipole moments. In contrast, even when the exciton interaction is negligible, the charge-transfer interactions are applied when the distance between the constituting units is short. In such molecules, the MO method is effective. Here, we describe the MMLCT excited state using Pt(II) diimine complexes as a typical example [8]. When Pt(II) diimine complexes form aggregates or crystalline states with a close contact between Pt(II) ions, the electronic absorption band and luminescence are observed at longer wavelengths (Fig. 3.8). This is explained by the formation of the σ and σ^* orbitals due to the interaction between the d_z^2 orbitals of Pt ions, and the transition from the σ^* orbital to the π^* orbital of the diimine ligand appears on the lower energy side (longer wavelength side) (Fig. 3.9). This ($\sigma^*-\pi^*$) is called as MMLCT, which is a crucial photophysical property in molecular crystals consisting of integrated metal complexes.

3.6 Photophysical Properties of Molecular Crystals

As described in Sect. 3.5, there are two methods, i.e., VB and MO methods, for understanding the photophysical properties of dimers or oligomers. The MO method leads to the band theory, wherein the valence and conduction bands are formed as a results of the interactions between the HOMOs of constituents and those between

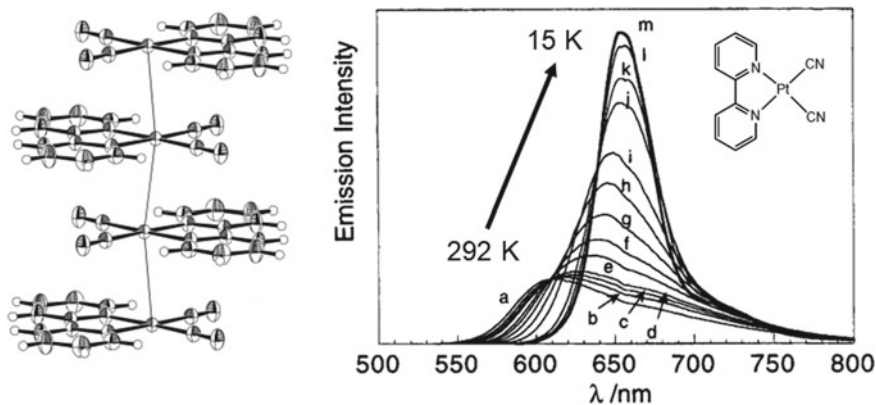
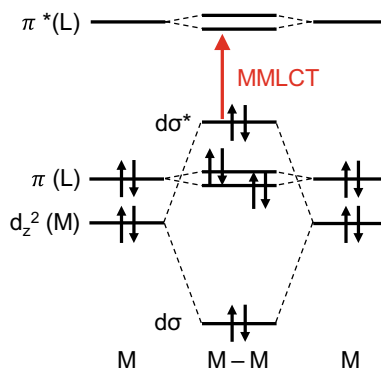


Fig. 3.8 Stacking structure of the red form of [Pt(bpy)(CN)₂] and the ³MMLCT emission spectra at different temperatures: a 292, b 260, c 240, d 220, e 180, f 160, g 140, h 120, I 100, j 60, k 45, l 30, m 15 K [8]

Fig. 3.9 Explanation of the MMLCT transition using the molecular orbital diagram of the dimer model



the LUMOs of constituents, respectively. This approach is useful for discussing the conductivity of crystals but it has a disadvantage of difficulty about the direct comparison of the band theory with the photophysical properties of molecular monomers, which have been accumulated by the spectroscopic measurements of molecules in solution and their theoretical calculations. Thus, for instance, the MMLCT luminescence observed in the molecular crystal of a metal complex is explained by the MO method, using the comparison between the monomer and the dimer. In contrast, the VB method is based on the photophysical properties of molecular monomers and takes into account exciton and charge-transfer interactions as the intermolecular interactions, although it is weak to correctly consider the strong intermolecular interactions. Thus, historically, Davydov splitting, which reflects exciton interaction, had been developed as the first theoretical approaches for explaining the spectral broadening of molecular crystals.

In this section, in order to show the example connecting between the monomer to the molecular crystals, we briefly illustrate the VB method-based analyses on photophysical properties of oxotitanium phthalocyanine (OTiPc) crystals, including both exciton and charge-transfer interactions [10]. OTiPc forms a few crystal structures, i.e., crystal polymorphisms such as phases I, II, and Y (phases I and II are also called β and α phases, respectively). One of them, phase II, has been practically utilized as near-infrared light-active photoconductors in GaAsAl laser printers and photocopiers because their photoconductivities are highly dependent on their crystal structures. Also, in contrast to the sharp Q absorption band in solution, the electronic absorption spectra of OTiPc thin films are significantly broadened and shift to longer wavelength side; the broadening and red-shift are dependent on the crystal structures.

The electronic absorption spectra of OTiPc thin films in phases I and II are shown in Fig. 3.10. In phase I, a broad absorption band between 650 and 800 nm is observed, whereas in phase II, it exceeds 800 nm. The electroabsorption measurements indicated that the charge transfer band was assigned to the 800 nm-region for the thin films in the phases II and Y. In the charge transfer band, the mixture of the exciton and charge-transfer configurations is essential; the absorbance of the charge-transfer band is caused by a contribution of the transition electric dipole-allowed exciton configuration, while the magnitude of the charge-transfer character correlates with the photocurrent and photocharge generation efficiency.

After molecular orbital calculations and configuration interactions for each molecule, the photophysical properties of OTiPc crystals are theoretically calculated by considering the exciton and charge-transfer electron configurations as intermolecular interactions. The theoretical calculations demonstrate that (1) the large red-shift in phase II is caused by the exciton interaction between OTiPc constituents, and (2) the

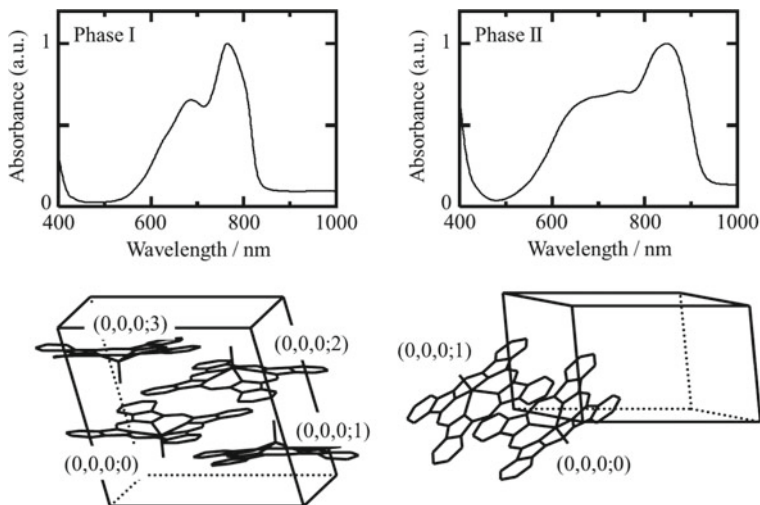


Fig. 3.10 UV-vis absorption spectra of OTiPc crystals in phases I (left) and II (right) and their crystal structures [10]

charge transfer band and the high photoconductivity observed in phase II are highly dependent on the intermolecular resonance integrals, which are well-correlated with the orbital overlaps. In other words, the electronic absorption spectroscopic properties can be tuned by manipulating the excitation energy of constituting molecules and the exciton interactions between constituents. Further, the design of molecular crystals to increase the intermolecular resonance integrals is crucial for achieving high photoconductivity.

References

1. Kato M, Ito H, Hasegawa M, Ishii K (2019) *Chem Eur J* 25:5105–5112
2. Davydov AS (1964) *Sov Phys Usp* 7:145–178
3. Turro NJ (1991) *Modern molecular photochemistry*. University Science Books, New York
4. (a) Ishii K, Kobayashi N (2003) *The porphyrin handbook*, eds Kadish K, Smith RM, Guillard R, vol 16. Academic Press, San Diego, pp 1–42. (b) Ishii K, Kitagawa Y (2014) *Handbook of porphyrin science*, vol 32, ed by Kadish K, Smith RM, Guillard R. World Scientific Publishing, Singapore, Chapter 168, pp 173–270. (c) Miwa H, Ishii K, Kobayashi N (2004) *Chem Eur J* 10:4422–4435
5. (a) Wang M, Ishii K (2022) Photochemical properties of phthalocyanines with transition metal ions. *Coord Chem Rev* 468:214626. (b) Ishii K, Shiine M, Shimizu Y, Hoshino S, Abe H, Sogawa K, Kobayashi N (2008) *J Phys Chem B* 112:3138–3143.
6. (a) Ishii K, Yamauchi S, Ohba Y, Iwaizumi M, Uchiyama I, Hirota N, Maruyama K, Osuka A (1994) *J Phys Chem* 98:9431–9436. (b) Ishii K, Ohba Y, Iwaizumi M, Yamauchi S (1996) *J Phys Chem* 100:3839–3846. (c) Ishikawa N, Ohno O, Kaizu Y, Kobayashi H (1992) *J Phys Chem* 96:8832–8839
7. Bilsel O, Rodriguez J, Milam SN, Corlin PA, Girolami GS, Suslick KS, Holten D (1992) *J Am Chem Soc* 114:6528–6538
8. Kato M (2007) *Bull Chem Soc Jpn* 80:287–294
9. (a) Ishii K, Sakai N (2010) *Phys Chem Chem Phys* 12:15354–15357. (b) Oddos-Marcel L, Madeore F, Bock A, Neher D, Ferencz A, Rengel H, Wegner G, Kryschi C, Trommsdorff HP (1996) *J Phys Chem* 100:11850–11856
10. (a) Nakai K, Ishii K, Kobayashi N, Yonehara H, Pac C (2003) *J Phys Chem B* 107:9749–9755. (b) Saito T, Sisk W, Kobayashi T, Suzuki S, Iwayanagi T (1993) *J Phys Chem* 97:8026–8031. MM+

Open Access This chapter is licensed under the terms of the Creative Commons Attribution 4.0 International License (<http://creativecommons.org/licenses/by/4.0/>), which permits use, sharing, adaptation, distribution and reproduction in any medium or format, as long as you give appropriate credit to the original author(s) and the source, provide a link to the Creative Commons license and indicate if changes were made.

The images or other third party material in this chapter are included in the chapter's Creative Commons license, unless indicated otherwise in a credit line to the material. If material is not included in the chapter's Creative Commons license and your intended use is not permitted by statutory regulation or exceeds the permitted use, you will need to obtain permission directly from the copyright holder.

